Nicotinic actions on neurones of the central autonomic area in rat spinal cord slices

A. Bordey, P. Feltz and J. Trouslard*

Laboratoire de Neurophysiologie et Neurobiologie des Systèmes Endocrines, URA CNRS 1446, Université Louis Pasteur, 21 rue René Descartes, 67084 Strasbourg Cedex, France

1. Nicotinic responses and actions on excitatory synaptic activity were studied in eighty-four neurones in the region dorsal to the central canal (lamina X) in transverse thoracolumbar spinal cord slices of neonate (P2–P10) rats by using the whole-cell patch-clamp technique.

2. Neurones ($n = 15$) labelled with Lucifer Yellow, showed the typical morphology of sympathetic preganglionic neurones (SPNs) in the central autonomic area (CA). Unlabelled neurones of comparable morphology were visually identified and recorded.

3. All neurones recorded responded to the nicotinic acetylcholine receptor (nAChR) agonist, DMPP. Under current-clamp conditions, pressure ejections of DMPP depolarized cells and induced the discharge of action potentials. Tetrodotoxin suppressed action potentials but not DMPP-induced depolarization.

4. Under voltage-clamp conditions at a holding potential (V_h) of −50 mV, DMPP induced a transient inward current (which reversed around 0 mV) and an increase in membrane current noise in 50% of the recorded neurones. In the others, DMPP increased membrane current noise without measurable inward current. The current–voltage relationship showed strong inward rectification at holding potentials more positive than 0 mV.

5. In neurones displaying a detectable current response to DMPP, the following agonist rank order potency could be established: DMPP = nicotine > cytisine > ACh. The DMPP response could be blocked by mecamylamine but was insensistive to methyllycaconite.

6. Pressure application of glutamate induced inward currents in all cells tested at a V_h of −50 mV. This response reversed at 10 mV, displayed a region of negative slope conductance at V_h more negative than −30 mV and was partially blocked by CNQX. Pressure application of DMPP transiently increased the amplitude of the glutamate-induced current in six out of nine cells tested. This potentiation persisted in the presence of tetrodotoxin.

7. Forty per cent of the recorded neurones displayed spontaneous excitatory postsynaptic currents (sEPSCs). At a V_h of −50 mV the sEPSCs had a mean amplitude of −19·3 pA and occurred at a frequency below 0·5 Hz. sEPSCs were blocked by CNQX and inverted around 0 mV. Brief application of DMPP increased the discharge frequency of sEPSCs without affecting their kinetics. Additionally, in some cells DMPP increased mean sEPSC amplitude.

8. Focal electrically evoked EPSCs reversed close to 10 mV and were sensitive to CNQX. They occurred with a constant latency, rise time and a mono-exponential decay time. Application of DMPP decreased the percentage of stimulation failures and increased the amplitude of evoked EPSCs, in all cells tested.

9. It is concluded that neurones in the CA, presumed to be SPNs, have functional nAChRs with activation having two distinct effects: firstly, a direct depolarization of the postsynaptic membrane; and secondly, a facilitation of the excitatory transmission onto these cells. This second effect is achieved by an increase of the size of the glutamate-induced current at the postsynaptic level as well as by an enhancement of the presynaptic release of glutamate.

* To whom correspondence should be addressed.

Sympathetic preganglionic neurones (SPNs) subserve a large subset of autonomic reflexes and are located in the thoracic and upper lumbar spinal cord. They receive inputs from multiple afferent sources, which are either of supraspinal origins or intrinsic to the spinal cord (for review, see Coote, 1988). In mammals, most SPNs are located in the intermediolateral cell column (IML), in the adjacent lateral funiculus and in the nucleus intercalatus. The fourth nucleus of the autonomic spinal network is the central autonomic area (CA), also called intermediomedial nucleus (Coote, 1988; Hosoya, Nadelhaft, Wang & Khono, 1994). Whilst most physiological studies have focused on SPNs in the IML, the properties of SPNs in the CA are not well documented.

Intrinsic cholinergic neurones are widely distributed in the spinal cord but are mainly in the lamina X. Some of these neurones are considered to be propriospinal in nature (Barber, Phelps, Houser, Crawford, Salvaterra & Vaughn, 1984; Borges & Iversen, 1986) and have been shown to make synaptic contacts onto neurones in the CA (Sherrif & Henderson, 1994). SPNs in the CA are thus well placed to be influenced by these propriospinal cholinergic neurones and may possess cholinergic receptors themselves. Indeed, mRNAs for various subunits of the nicotinic acetylcholine receptors (nAChRs) have been detected in the spinal cord by *in situ* hybridization studies (Wada *et al.* 1989). However, the functional presence of nAChRs on SPNs still remains controversial (Coote, Macleod, Fleetwood-Walker & Gilbey, 1981; Yoshimura & Nishi, 1982; Khan, Taylor & Yaksh, 1994*a*; Khan, Yaksh & Taylor, 1994*b*).

In the present study, the effects of nAChRs agonists were examined on visually chosen neurones of the CA in transverse rat spinal cord slices with whole-cell patch-clamp recordings. We show the presence of functional nAChRs on these neurones presumed to be SPNs according to their location and morphology. Activation of the nAChRs increased firing and enhanced glutamate-evoked currents. In addition, we show that ACh acts presynaptically on the recorded neurones to facilitate excitatory synaptic transmission.

METHODS

Slice preparation

The method for the preparation of thin spinal cord slices used in this study was as previously described by Krupp & Feltz (1993). Neonate (postnatal days, P2–P10) Wistar rats were decapitated under deep diethylether anaesthesia. The spinal cord was removed and transverse slices (T3–L3; 200–250 μm) were cut using a Vibratome (Oxford Vibratome Series G). Slices were transferred to a storage chamber containing sucrose-based artificial cerebrospinal fluid (ACSF, see below for composition) and maintained at room temperature (20–22 °C). After recovery of 1 h, a slice was transferred to the recording chamber and held in position by a nylon mesh glued to a U-shaped platinum wire. The recording chamber was superfused at a rate of 2 ml min^{-1} with oxygenated ACSF at 33 °C.

Solutions

The ACSF used contained (mM): NaCl, 113; KCl, 3; NaH_2PO_4, 1; $NaHCO_3$, 25; glucose, 11; $CaCl_2$, 2; $MgCl_2$, 1. The sucrose-based ACSF used during the dissection procedure contained (mM): sucrose, 248; KCl, 2; KH_2PO_4, 1·25; $NaHCO_3$, 26; glucose, 11; $CaCl_2$, 2; $MgSO_4$, 2. Both ACSFs had a pH of 7·4 when bubbled with 95% CO_2–5% O_2. The intracellular solution used consisted of (mM): potassium gluconate, 140; $MgCl_2$, 1; MgATP, 1; Hepes, 10; EGTA, 10; $CaCl_2$, 1; pH 7·3 (adjusted with NaOH). Lucifer Yellow (lithium salt) was added to the internal solutions at a final concentration of 1·5 mg ml^{-1}.

Drugs and application systems

All drugs were purchased from Sigma except methyllycaconitine, which was obtained from Research Biochemicals International. Drugs were diluted in ACSF and applied to the slice by superfusion. Acetylcholine, muscarine, 1,1-dimethyl-4-phenyl-piperazinium (DMPP), cytisine and nicotine were applied by a computer-controlled pressure-ejection system. The pressure-ejection pipettes were standard unpolished patch electrodes with resistances of either 6–8 MΩ for local nAChR agonist application (for studying postsynaptic nicotinic responses) or 4–6 MΩ for more diffuse nicotinic agonist application (for studying the effects of agonist applications on the synaptic activity). The pressure-ejection pipette was located just above the slice at a distance of 20–30 μm from the recorded cell for local application and at a distance of 50–60 μm from the recorded cell, for more diffuse application. Pressure ejection of control ACSF (without agonist) produced no response (data not shown). When the potency of two agonists were compared, we used two pressure pipettes, each filled with a different agonist. These pipettes were located equidistant from the recorded cell. When the two pressure pipettes were filled with the same agonist, the application of agonist from either of the two pipettes induced currents with similar amplitudes and kinetics.

Recording conditions, stimulation and analysis

Slices were observed under Nomarski optics using an upright microscope (Zeiss Axioskop FS) equipped with a × 40 water immersion objective (Zeiss, Germany). Patch pipettes were pulled on a L/M-3P-A puller (List Electronics, Darmstadt, Germany) from microfilament-filled borosilicate glass (o.d., 1·55 mm; wall thickness, 0·35 mm; Phymep, Paris). For whole-cell recordings, patch electrodes were filled with intracellular solution (see above) and had resistances of 4–6 MΩ. A high positive pressure was applied to the patch pipette. This positive pressure facilitated the cleaning of the slice and the sealing of the pipette onto the visually chosen neurone. Whole-cell voltage-clamp recordings were performed using an Axopatch-2A amplifier (Axon Instruments). The capacitance and leak current were evaluated by applying negative rectangular potential steps (−20 mV). The resulting membrane current charging curves were fitted with the sum of two exponentials (Llano, Marty, Armstrong & Konnerth, 1991) which allowed calculation of: the pipette-access resistance (R_1); the corresponding somatic and proximal dendritic capacitance (C_1); the resistance (R_2) which linked the main dendrites to each distal dendrite; and the corresponding capacitance (C_2). The pipette-access resistance, R_1, was 9·6 ± 1·6 MΩ ($n = 21$) and R_2 was 8·9 ± 3·2 MΩ ($n = 21$). The capacitance, C_1, was 82 ± 6·2 pF and C_2 was 131·7 ± 8·0 pF ($n = 21$). Focal stimulation of fibres in the lamina X of the spinal cord was achieved using patch pipettes filled with ACSF (2–3 MΩ) normally positioned in a sphere of 50–60 μm away from the cell in any direction. Stimuli (100 μs, 5–40 V) were generated by a stimulation-isolation unit and usually delivered at 1 Hz.

Signals were stored on magnetic tape (Racal recorder, UK) with a bandwidth of 2·5–10 kHz and in a Hewlett-Packard Vectra computer in combination with pCLAMP 5·5 software (Axon Instruments) operating a data acquisition board (Labmaster, 40 kHz DMA). Signals were filtered at 1–2 kHz (4-pole Bessel filter) and digitized at 4–5 kHz, except for capacitance and action potential analysis, where signals were filtered at 5 kHz and digitized at 10 kHz. The rise time and the amplitude or height of the action potentials were measured from the firing threshold (the point of onset of the rising phase of the action potential) to the peak of the action potential. The amplitudes of after-hyperpolarization were also measured with respect to the firing threshold. The spike width was measured at threshold and at half-height. Each value represents the mean of ten action potentials per cell. The criteria used for counting spontaneous, DMPP induced and evoked excitatory postsynaptic currents (EPSCs) were responses with an amplitude greater than 5 pA and a rise time shorter than 3 ms. The amplitude of spontaneous and evoked EPSCs and the latency of evoked EPSCs were measured as the difference between a first cursor placed at the beginning of the stimulation artefact and a second cursor placed at the onset or at the peak of the response. Mean amplitude and kinetic parameters of spontaneous and evoked EPSCs are calculated from twenty to forty synaptic events in each cell before and after DMPP application.

Results are expressed as means ± S.E.M. with n being the number of cells tested. The differences between control and test conditions were tested for significance using Student's t test ($P < 0·001$).

Examination of cell morphology

Cells were recorded from depths of 20–80 μm into the slice. Neurones visually chosen for recordings were photographed using a closed-circuit television camera (Sanyo, Japan) and Biocom software (Biocom, Les Ulis, France) for later analysis of the location and somatic morphology. When recorded cells had been filled with Lucifer Yellow, slices were transferred to a fixing medium (4% paraformaldehyde with 0·1 mM phosphate buffer) and stored overnight in the refrigerator. The slices were cleared on the following day for 10 min in dimethyl sulphoxide (Grace & Llinas, 1985), mounted on microslides in a Sigma Diagnostics mounting medium and covered with coverslips. After mounting, the slices were examined under epifluorescent illumination, using a Zeiss filter combination (bandpass filter for excitation, 450–490 nm; bandpass filter for emission, 515–565 nm) for Lucifer Yellow fluorescence and photographed.

RESULTS

Identification of cells

Cells filled with Lucifer Yellow ($n = 15$; Fig. 1) or observed with Biocom software ($n = 16$) were located in a position dorsal to the central canal (Fig. 1). They had either round- or oval-shaped somata with their long axis orientated mediolaterally. The cell size ranged from 19·5 × 9 to 25 × 16·5 μm ($n = 31$). Stained cells had three to four dendrites extending medially towards the commissure and central canal and laterally towards the intermediate grey matter. Dendrites had a beaded appearance due to the occurrence of varicosities, as observed in previous studies of SPNs in the intermediolateral cell column (IML; Krupp & Feltz, 1993). The axon was thinner and less beaded than the dendrites and extended either from the soma or the main proximal dendrites ($n = 7$). This morphology was shown to be typical for SPNs of the CA (Barber *et al.* 1984; Hosoya *et al.* 1994).

Recordings were obtained from eighty-four visually chosen cells located in the area dorsal to the central canal. They had a mean resting membrane potential of −54·6 ± 1·5 mV (ranging from −45 to −62 mV, $n = 12$) and a mean input resistance of 382·4 ± 42·1 MΩ (ranging from 125 to 800 MΩ, $n = 20$). These values were obtained in the first 3 min of whole-cell recording. All cells fired action potentials in response to a depolarizing current injection, but were also seen to fire spontaneously. During the first 10 min of recording the spike frequency decreased either from 4–6 Hz to 1–2 Hz in cells with a high basal activity or from 1–2 Hz to quiescence in cells with a lower basal activity. The decrease in the spike frequency was not due to a change in the input resistance and was not accompanied by a change in the membrane current. In the ten cells studied at −60 mV: the threshold for firing was −46·5 ± 2·3 mV; the spikes had a rise time of 1·31 ± 0·09 ms; an amplitude of 62·2 ± 3·3 mV; a half-duration of 1·66 ± 0·12 ms; a total duration of 3·29 ± 0·23 ms; and an overshoot of 23·1 ± 1·1 mV.

DMPP responses

DMPP was first tested in the current-clamp configuration. Cells displaying a response under current-clamp mode were further studied under voltage-clamp conditions. All the neurones tested responded to DMPP ($n = 84$).

In current-clamp mode, pressure ejection of DMPP (1 mM) during 5 s on four quiescent cells (no action potentials at resting potential) induced a depolarization which was accompanied by a 30 s long tonic discharge of action potentials up to a maximal frequency of 14 Hz (Fig. 2*A*). Brief (100 ms) applications of DMPP to a firing neurone enhanced the discharge frequency from 1–2 Hz to 4–6 Hz ($n = 6$). The DMPP-induced depolarization persisted in the presence of TTX (1 μM; $n = 3$) which blocked spike firing (Fig. 2*B*).

Under voltage-clamp conditions at −50 mV, a 100 ms pressure pulse of DMPP induced a small inward current (−16·3 ± 2·3 pA; $n = 16$) and an increase in membrane current noise. In fourteen cells only an increase in membrane current noise was evident and a DMPP-induced inward current was hardly measurable. The size of the DMPP-induced current depended on the membrane potential (Fig. 2*C*). The current–voltage relationship (Fig. 2*C*) gave an extrapolated reversal potential between −20 and 0 mV ($n = 5$ cells), compatible with a non-selective cationic current. Moreover this I–V relationship had a strong inward rectification since no current was observed for positive holding potentials up to +40 mV ($n = 5$). The amplitude of the current often declined during the recording with little or no reversibility even with ATP in the pipette solutions and when using short (100 or 500 ms) and infrequent (one pulse every 2 min) DMPP applications.

Pharmacological profile of the DMPP responses

The study of the pharmacological profile of nAChRs was restricted to neurones displaying a detectable inward current in response to the application of DMPP. In these cells, DMPP responses were compared with acetylcholine, nicotine and cytisine reponses as described in Methods (Fig. 3*A*). Cells were challenged with two successive control DMPP applications followed by an application of another nicotinic agonist and finally by a subsequent DMPP application. All applications were spaced at 3 min intervals. Cells which showed a marked run-down of the DMPP response were discarded. The amplitude of the cytisine- and acetylcholine-induced current was 30·9 ± 1·9% ($n = 4$) and 57·0 ± 1·3% ($n = 4$) of the DMPP current, respectively.

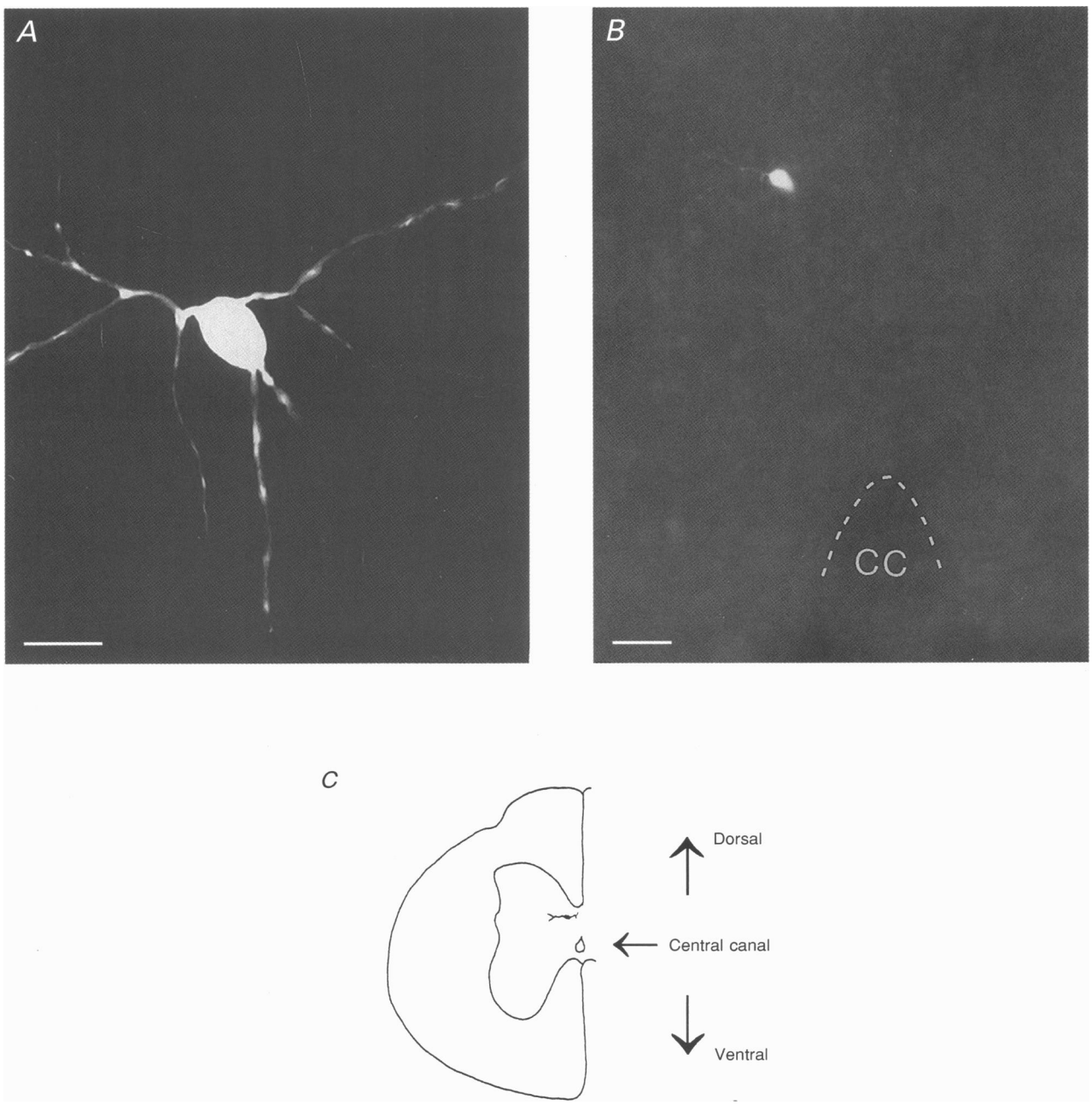

Figure 1. Photo montage showing a Lucifer Yellow-stained neurone

A, morphology of a neurone stained with Lucifer Yellow (1·5 mg ml^{-1}) in an upper lumbar (L1–L3) transverse rat spinal cord slice. This cell exhibits four main dendrites going laterally, medially and towards the central canal. Laterally and medially orientated dendrites divide into two branches along their length. Scale bar = 20 μm. *B*, the central autonomic area of the same cell as in *A*, photographed at lower magnification. The dashed line delineates the central canal (CC). Scale bar = 40 μm. *C*, schematic representation of the upper lumbar transverse spinal cord slice showing the location of the neurone displayed in *A* and *B*.

Nicotine-induced currents had comparable amplitude sizes to those of DMPP-induced currents ($n = 3$) but showed a partial recovery during the time of recording (Fig. 3*A*). Muscarine, a muscarinic AChR agonist, did not induce any detectable current ($n = 3$).

Several antagonists of nAChRs were tested either in voltage- or current-clamp conditions. *d*-Tubocurarine applied for 3 min (dTC; 100 μM; $n = 3$) and mecamylamine applied for 3–4 min (10 μM; $n = 3$) completely blocked the nicotinic response (Fig. 3*B*) in a partially reversible manner during

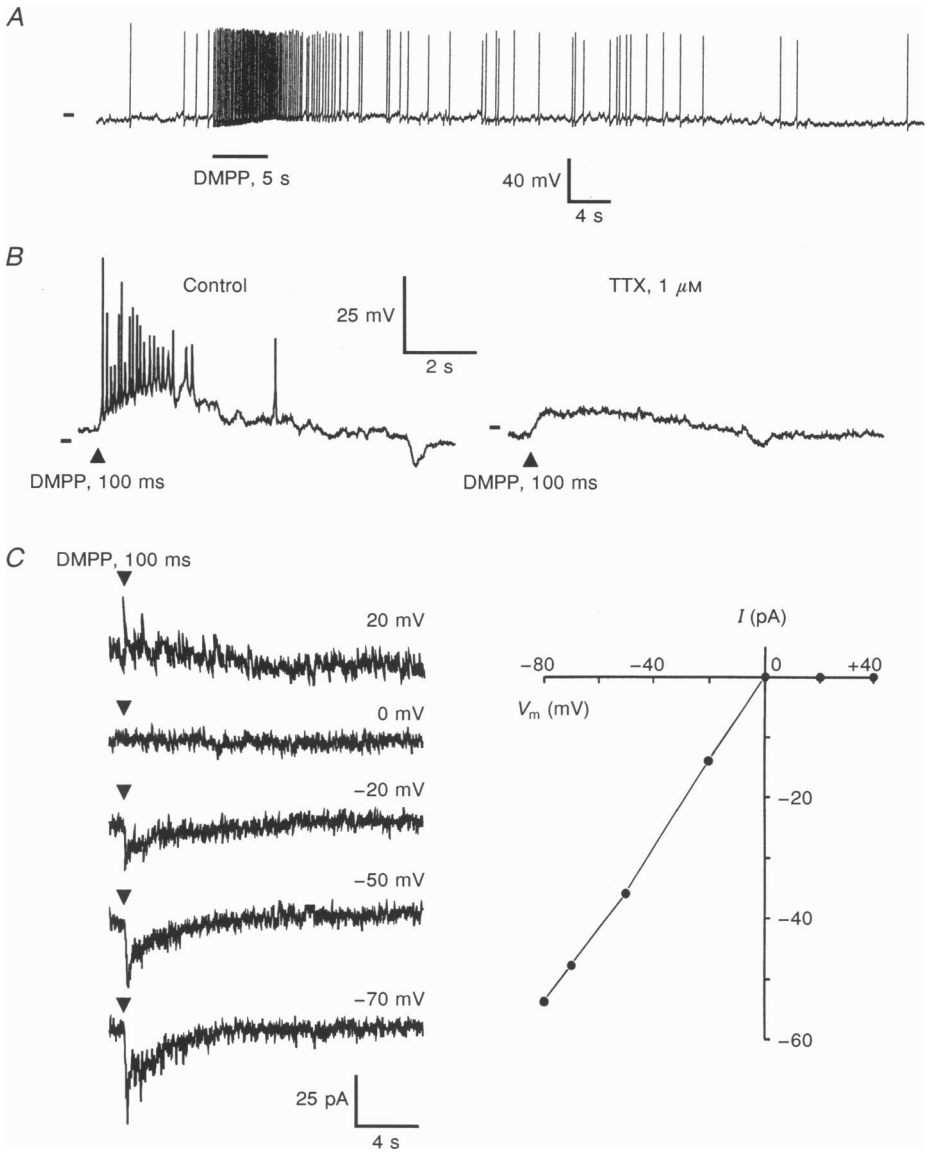

Figure 2. Effects of DMPP on neurones of the central autonomic area

A, under current-clamp conditions, DMPP (1 mM; 5 s) was applied by pressure ejection and induced a tonic discharge of action potentials which lasted more than 30 s. DMPP was applied during the time indicated by the horizontal bar. The resting membrane potential, as indicated by the bar at the beginning of the trace, was −60 mV. The spikes seen prior to the application of DMPP are due to a previous application of DMPP. *B*, under current-clamp conditions, pressure application of DMPP (1 mM) for 100 ms induced a depolarization on which spikes are superimposed. Superfusion of the slice by TTX (1 μM) for 6 min, abolished spiking activity without affecting the DMPP-induced depolarization without spikes. Spikes were truncated due to filtering during the digitization of the data. The bars at the beginning of the traces indicate the resting membrane potential of −70 mV. *C*, left panel: under voltage-clamp conditions, DMPP responses were recorded at different holding membrane potentials. DMPP was applied by pressure injection (1 mM; 100 ms). The peak amplitude of the current was measured and plotted against the membrane potential (V_m) in the right panel. Inspection of the *I–V* relationship indicated a reversal potential of the DMPP-induced current close to 0 mV and a strong inward rectification above 0 mV.

the time of recording. None of hexamethonium (50 μM, 10 min, $n = 5$, Fig. 3*B*); a classical ganglionic antagonist, methyllycaconitine (MLA, 100 nM, 10–20 min, $n = 3$, Fig. 3*B*); a specific antagonist of the α-bungarotoxin (α-BuTX)-sensitive nAChR (Alkondon, Pereira, Wonnacott & Albuquerque, 1992); and a neuronal κ-bungarotoxin (100 nM, 10–20 min, $n = 4$) abolished the DMPP-induced depolarization.

Actions of nicotinic agonists on currents induced by exogeneously applied glutamate

At a V_h of −50 mV, pressure application of glutamate (1 mM, 100–300 ms) induced an inward current in all cells tested ($n = 13$) that persisted in the presence of TTX (1 μM, $n = 3$). The size of the glutamate-induced current depended on the membrane potential (Fig. 4*A*). The current–voltage relationship (Fig. 4*B*) gave a reversal potential of 10·2 ± 5·4 mV ($n = 5$). Moreover this *I–V* relationship had a region of negative slope conductance at holding potentials more negative than −30 mV. Superfusion of 6-cyano-7-nitroquinoxaline-2,3-dione (CNQX; 10 μM) at −50 mV resulted in a 72·4 ± 2·6% ($n = 4$) block of the glutamate-induced current which suggests the involvement of both NMDA and non-NMDA components.

To investigate the DMPP effect on glutamate-induced currents, pressure applications of glutamate (1 mM, 200–300 ms) were made every 30 s and were then preceded by a pressure application of DMPP (1 mM; 5 s) just prior to the glutamate pulse. The glutamate-evoked currents after the application of DMPP were measured from the start of the glutamate response itself. DMPP considerably increased the glutamate-induced current in six out of nine cells tested (Fig. 4*C*). The peak amplitude of the glutamate-induced current immediately (2 or 3 s) after a DMPP application was increased to 174·3 ± 29·0% ($n = 6$) of the control level (mean amplitude of four or five glutamate-induced currents prior to the DMPP application). This potentiation persisted in the presence of TTX (1 μM; $n = 3$) and may thus be mediated by a postsynaptic nicotinic modulation of the glutamate response.

Actions of nicotinic agonists on spontaneous excitatory synaptic activity

At a V_h of −50 mV, about 40% of the recorded cells displayed spontaneous excitatory postsynaptic currents (sEPSCs; inward in our recording conditions) having a mean amplitude of −19·3 ± 3·3 pA ($n = 6$). sEPSCs occurred at a low and stochastic frequency below 0·5 Hz. At positive

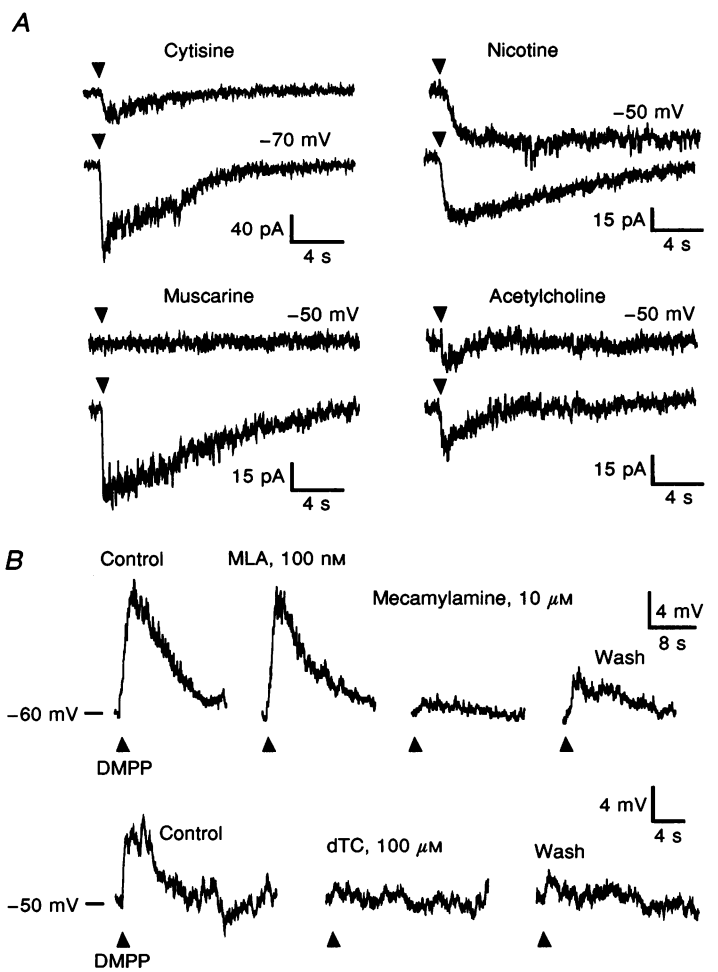

Figure 3. Pharmacology of the nicotinic response

A, responses to different nicotinic and muscarinic agonists were compared with DMPP responses in the same cell (see Methods). Each pair of traces consists of a test agonist-induced membrane current (upper trace) and for comparison a membrane current evoked by DMPP (lower trace). All drugs were applied by pressure at 1 mM for 500 ms at ▼. The holding potential is indicated for each pair of traces. *B*, antagonism of the DMPP-induced responses. Upper traces: DMPP-induced current was not affected by bath application of 100 nM MLA for 10 min. MLA was washed for 20 min and mecamylamine (10 μM) was applied for 4 min. Mecamylamine blocked the current in a partially reversible manner after 20 min wash-out. Holding potential was −60 mV. Lower traces: DMPP-induced currents (▲) in control (left), in presence of dTC (3 min, 100 μM, middle trace) and after 10 min wash-out of dTC. Holding potential was −50 mV.

holding potentials sEPSCs displayed a long-lasting outward current (Fig. 5*A*) which suggested a NMDA receptor-mediated component of the sEPSCs. The *I–V* relationship (Fig. 5*A*) of the peak amplitude of the sEPSCs ($n = 3$) was linear and had a reversal potential around 0 mV suggesting a non-selective cationic conductance for these sEPSCs. No outward rectification was seen in the *I–V* relationship because the peak currents measured were likely to be predominantly a non-NMDA receptor-mediated effect. At −50 mV, both spontaneous and DMPP-induced synaptic activity (see below) were completely blocked by superfusion of CNQX (10 μM, $n = 3$; Fig. 5*B*).

In all cells tested ($n = 12$) brief pressure application of DMPP (100 ms to 1 s) induced the appearance of or increased the discharge of sEPSCs as illustrated in Fig. 5*C*. In a subset of cells ($n = 4$), DMPP produced no change in the sEPSC amplitude compared with the situation before or after the DMPP application (upper trace of Fig. 5*C*; Student's *t* test, $P > 0{\cdot}001$). In another subset of cells ($n = 3$; lower trace of Fig. 5*C*), the mean sEPSC amplitude was increased to $136{\cdot}0 \pm 4{\cdot}2\%$ of its original amplitude. There was no significant change in either the rise time or the decay time between spontaneous and DMPP-induced EPSCs ($P > 0{\cdot}001$). At a V_h of −50 mV, spontaneous EPSCs measured in three cells had a rise time of $0{\cdot}67 \pm 0{\cdot}06$ ms and a mono-exponential decay time constant of $1{\cdot}63 \pm 0{\cdot}44$ ms. In the same three cells, DMPP-induced EPSCs measured during the first 30 s after the DMPP application had a rise time of $0{\cdot}65 \pm 0{\cdot}11$ ms and a mono-exponential decay time constant of $1{\cdot}55 \pm 0{\cdot}48$ ms. These unchanged kinetics of the EPSCs ($P > 0{\cdot}001$) suggest that there was no modification of the cable properties of the recorded cell. In addition the enhancement of the synaptic activity outlasted the DMPP-induced current by 30–60 s and was not accompanied by an increase in the conductance of the recorded cells when the conductance was monitored by applying negative pulses (−20 mV; data not shown).

Actions of nicotinic agonists on evoked excitatory synaptic activity

In six cells, electrical stimulation (see Methods) evoked monosynaptic EPSCs. In three of these cells held at a V_h of −50 mV, evoked EPSCs had a mean peak amplitude of

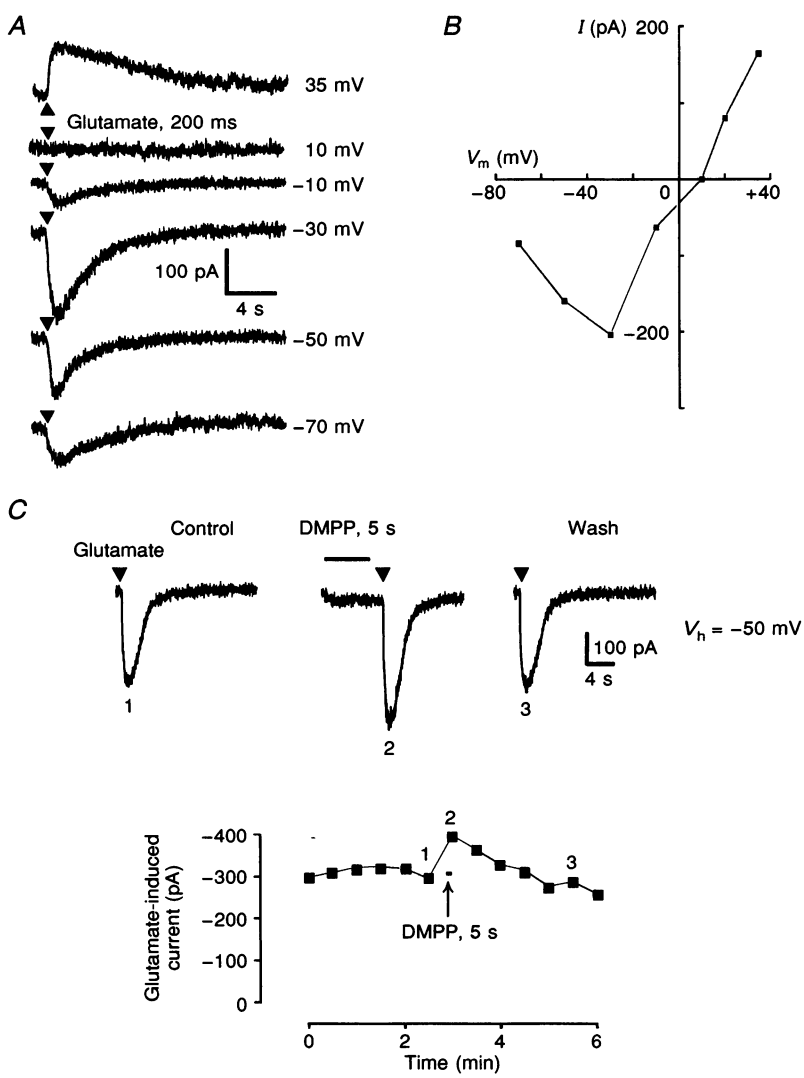

Figure 4. Potentiation by DMPP of the glutamate-evoked current

A, pressure application of glutamate (1 mM; 200 ms; ▲, ▼) elicited a transient inward current at the holding potentials indicated by each trace. The peak amplitude of this current was measured and plotted against the membrane potential in *B*. *B*, current–voltage relationship of the peak amplitude of the glutamate-induced current from the cell illustrated in *A*. The reversal potential of the glutamate-induced current is close to 10 mV; the *I–V* relationship shows a negative slope conductance at −30 mV. *C*, pressure applications of glutamate (1 mM; 200 ms, ▼) were performed every 30 s. The peak of glutamate-induced current was measured and plotted against time in the lower panel. Pressure application of DMPP (1 mM; 5 s) transiently increased glutamate-evoked current to 128% of the control value. Numbers 1, 2 and 3 refer to the current traces illustrated in the upper raw traces. The holding potential was −50 mV and TTX (1 μM) was present in the bath.

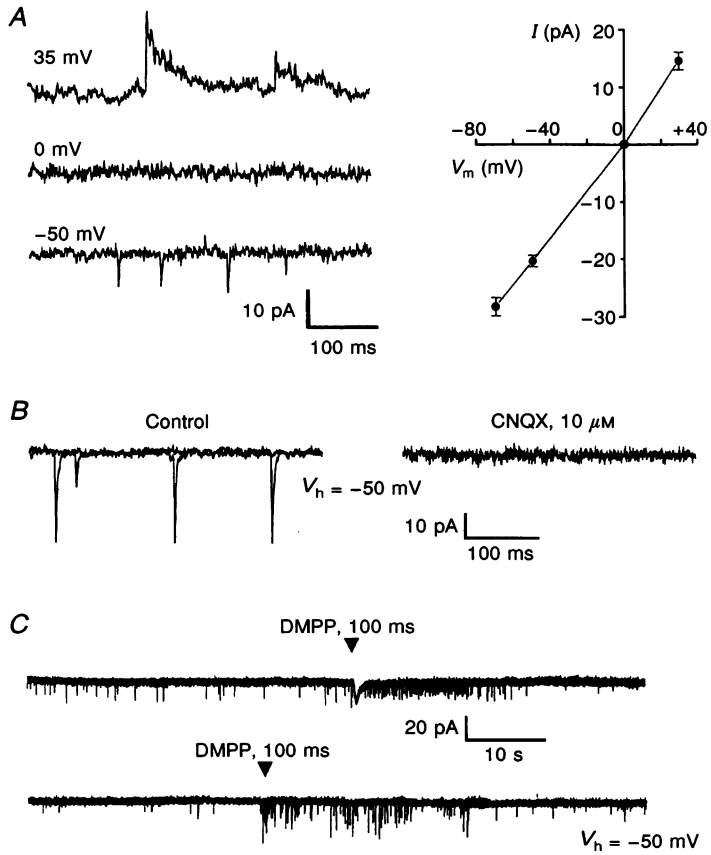

Figure 5. Spontaneous and DMPP-induced excitatory synaptic activity

A, in the left panel, voltage-clamp recordings of synaptic activity at the holding potentials indicated above each trace. Note that at 35 mV spontaneous EPSCs (sEPSCs) displayed a long-lasting outward current. The peak amplitude of sEPSCs were measured at different holding potentials. Data were collected from 3 cells (20–40 events in each cell for each potential) and mean results plotted against the holding potential in the right panel. The *I–V* relationship of the peak amplitude of the sEPSCs was linear and gave a reversal potential around 0 mV. *B*, two superposed current traces showing sEPSCs at −50 mV (left panel). As shown in the right panel, superfusion of CNQX (10 μM) for 10 min completely abolished the spontaneous EPSCs. *C*, in the upper trace, pressure application of DMPP (▼) induced a transient inward current and enhanced the frequency of the synaptic activity in SPNs without affecting the mean amplitude of the EPSCs (see text). In the lower trace, in another cell, DMPP (▼) increased both the frequency and the amplitude of the sEPSCs. DMPP (1 mM) was applied for 100 ms at the times indicated. Holding potential was −50 mV.

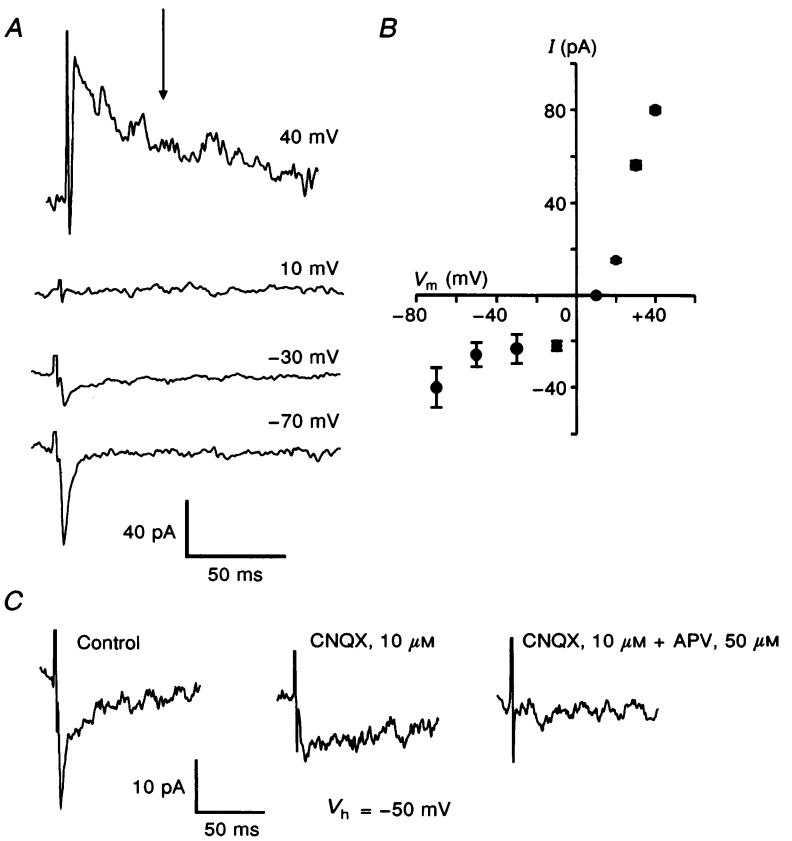

Figure 6. Excitatory synaptic activity evoked by electrical stimulation in lamina X

A, focally evoked EPSCs were recorded in a neurone held at different holding potentials indicated above each trace. Membrane depolarization revealed a slow component to the EPSC decay, as indicated by the arrow positioned 50 ms after the onset of the EPSC. The peak current amplitude was measured in 3 cells at different holding potentials (30 events for each cell and for each holding potential) and means plotted against the holding potential in *B*. *B*, current–voltage relationship of the peak amplitude of evoked EPSCs. The *I–V* plot gave a reversal potential around 10 mV and showed a strong outward rectification below −10 mV. *C*, EPSCs were evoked at a membrane potential of −50 mV before (Control, left trace) and 6 min after the addition of CNQX (10 μM) to the superfusing solution (middle trace). The subsequent addition of APV (50 μM) completely abolished the remaining response (right trace).

-26 ± 5 pA (stimulation of 20 V). They occurred with a latency of $2{\cdot}03 \pm 0{\cdot}41$ ms and had a rise time of $1{\cdot}41 \pm 0{\cdot}28$ ms (mean of 20–40 events in each cell). Their time course of decay could be fitted by a mono-exponential function with a time constant of $3{\cdot}26 \pm 0{\cdot}14$ ms ($n = 3$). Membrane depolarization revealed a second, slowly decaying component of the evoked EPSCs (Fig. 6*A*). *I–V* relationships for the peak amplitude of the evoked EPSCs had a reversal potential of $9{\cdot}6 \pm 3{\cdot}2$ mV and showed an outward rectification at membrane potentials more negative than -10 mV (Fig. 6*B*). At a V_h of -50 mV, the evoked EPSCs were completely blocked by CNQX (10 μM; $n = 2$) or by the combination of CNQX and DL-2-amino-5-phosphonovalerate (APV; 50 μM) in a third cell (Fig. 6*C*). These results suggest that evoked EPSCs are mediated by activation of both NMDA and non-NMDA receptors.

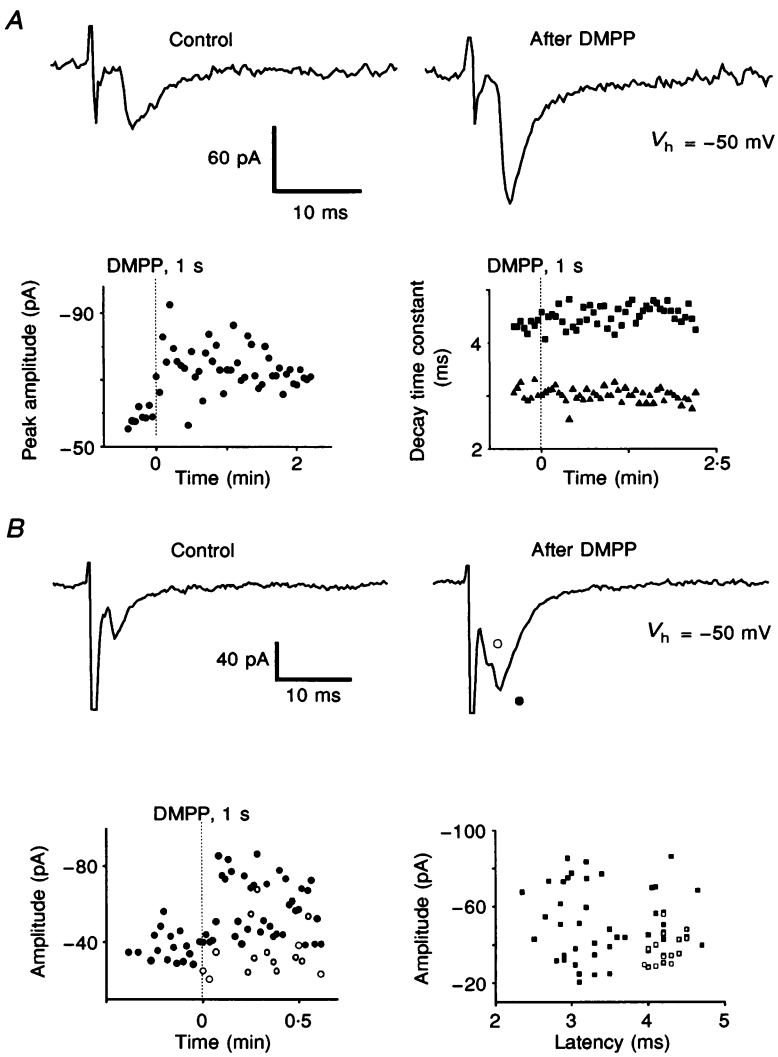

Figure 7. Potentiation of electrically evoked EPSCs by DMPP action

EPSCs were induced by electrical stimulation of lamina X at 1 Hz and the effect of pressure application of DMPP (1 mM; 1 s) was monitored on the amplitude, latency and decay time course of the evoked EPSCs. The holding potential was -50 mV. *A*, the upper panel displays typical recordings of evoked EPSCs in control (left trace) and 20 s after the DMPP application (right trace). The mean peak amplitudes of 5 successive evoked EPSCs (●) were plotted against time in the lower left panel. This graph showed that DMPP applied at time 0 induced a long lasting increase in the amplitude of the EPSC. In the lower right panel, the graph shows plots of the latency (▲) and mono-exponential decay time constant (■) of evoked EPSCs before and after DMPP application at time 0. No change of the latency and decay time constant was observed after the DMPP application. *B*, in this cell, DMPP increased the amplitude of electrically evoked EPSCs and induced the appearance of an additional EPSC with a shorter latency. Traces: the left trace illustrates a typical EPSC evoked before the application of DMPP. After the DMPP application electrical stimulation evoked EPSCs with a rise phase composed of at least two components. The amplitude of these two components was measured and plotted against time (left graph, ●, ○) and latency (right graph, □, ■). ○, events of shorter latency and ●, events of longer latency. □, ■ refer to events measured before and after DMPP application, respectively.

In all the cells tested ($n = 6$) pressure application of DMPP (1 mM; 1 s) increased the amplitude of the evoked EPSCs (Fig. 7*A* upper traces and left graph). Following the DMPP application, the peak EPSC amplitude was increased to 141·3 ± 8·8% of the control amplitude ($n = 4$ cells). The potentiation of evoked EPSCs recovered within 10–15 min. This potentiation of evoked EPSCs occurred in the absence of a significant increase in input resistance and was not associated with an obvious change in the kinetics of EPSCs (Fig. 7*A* right graph; $P > 0{\cdot}001$). After DMPP application, EPSCs displayed a latency of 1·78 ± 0·36 ms, a rise time of 1·39 ± 0·31 ms and a mono-exponential decay with a time constant of 3·20 ± 0·17 ms in the same three cells previously studied for the measurements of the EPSCs kinetic parameters. In another three cells showing a high percentage of failures (77·0 ± 11·8%), DMPP application decreased the number of failures to 33·2 ± 2·3%. This result supports the view that the DMPP-induced increase in evoked EPSCs amplitudes resulted from an enhancement of the presynaptic release of glutamate or an analogue substance.

In addition to the amplitude potentiation of evoked EPSCs, pressure application of DMPP resulted in the appearance of an inflexion in the rising phase of evoked EPSCs in two out of six cells tested (Fig. 7*B*) with no concomitant change in the decay time course. The left graph in Fig. 7*B* illustrates such a DMPP-induced appearance of an additional evoked EPSC with a shorter latency, likely to be due to the activation of a second, hitherto quiet synapse.

DISCUSSION

Identification of recorded neurones

We recently described a subpopulation of neurones located in the lamina X express nAChRs (Bordey, Feltz & Trouslard, 1996). The neurones described in the present study differ from those neurones in their morphology, location and nicotinic receptor pharmacology. Recorded cells were presumed to be SPNs according to their location in the CA and their morphology (Barber *et al.* 1984; Hosoya *et al.* 1994). Consistent with results of Barber *et al.* (1984) for SPNs of the CA, we found that the visually chosen cells for recording were more numerous at the upper lumbar level than at thoracic level. In addition, their electrophysiological properties were comparable to those previously described for SPNs of the IML (for review Coote, 1988; Inokuchi, Masuko, Chiba, Yoshimura, Polosa & Nishi, 1993).

Nicotinic AChRs mediate synaptic transmission in several parts of the brain. At the spinal cord level, nAChRs located on Renshaw cells play an important role in the recurrent inhibition of motoneurones by ACh (Eccles, Fatt & Koketsu, 1954). Since few reports have described an effect of nAChR activation within the spinal cord (Myslinski & Randic, 1977; Yoshimura & Nishi, 1982; Urban, Willetts, Murase & Randic, 1989; Perrins & Roberts, 1994), we have applied the patch-clamp technique to spinal cord slices of neonate rat and discovered that nicotinic agonists acting through the activation of nAChRs have complex stimulatory effects on presumed SPNs located in the CA. We have demonstrated that these neurones express nAChRs with activation leading to the induction of firing and the potentiation of glutamate responses. Moreover nAChR agonists act at the presynaptic level to facilitate the release of glutamate or an analogue substance. The function of this dual excitatory action of nicotinic agonists is discussed with respect to the role of SPNs and cholinergic interneurones in lamina X.

Postsynaptic actions of cholinergic agonists

Acetycholine binds to two classes of receptors, muscarinic and nicotinic. While muscarinic receptors are formed by a single protein coupled to a G protein, neuronal nAChRs are formed by the pentameric association of two classes of subunits, α and β, that form a non-selective cationic conductance. The cationic selectivity of the recorded currents and the nicotinic agonist and antagonist efficacy rule out the activation of muscarinic receptors. In addition, the actions of nAChR agonists were direct onto these neurones because the DMPP-induced current was unaffected by TTX which blocked neuronal conduction. In 50% of neurones, nAChR agonists induced an inward current of small amplitude (−15 pA at −50 mV), the other neurons only showed an increase in membrane current noise without measurable inward current. It is difficult to understand how such an increase in noise without detectable inward current is sufficient to depolarize the cell and induced firing. This could be explained by the the fact that any small current, even in the picoampere range, flowing through a high input resistance gives a significant depolarization. This initial depolarization might have activated other voltage-dependent conductances leading to a depolarization of sufficient size to induce firing of the cell. However, it is also possible that in neurones lacking detectable DMPP-induced currents, nicotinic receptors were still partially desensitized when DMPP was applied under voltage clamp which was always performed following the first application of DMPP under current clamp. This small current amplitude may explain why no previous study has reported nicotinic responses in SPNs (Coote *et al.* 1981). Only one study using conventional intracellular recordings found nicotinic responses and these were in only 57% of SPNs of the IML (Yoshimura & Nishi, 1982). In contrast, the high resolution of the patch-clamp technique has allowed us to detect these small currents. Several explanations could account for the small size of the nicotinic current. These neurones could possess only a few nAChRs, which correlates with the low density of binding sites for [^{3}H]cytisine and [^{3}H]nicotine found in spinal cord membrane preparations (Khan *et al.* 1994*b*). nAChRs could be mainly present on the dendritic processes extending in both the rostrocaudal and mediolateral directions. As the major part of the rostrocaudally oriented dendrites will be cut during the slice preparation, this would lead to a substantial loss of nAChRs. In addition, the nicotinic agonist concentration decreases dramatically through the depth of the slice and

could be insufficient to activate nAChRs located deep in the slice. However, this explanation is unlikely because we have recorded interneurones at the same depth in the slice which displayed nicotinic-induced current in the nanoampere range (Bordey *et al.* 1996).

Pharmacology. Molecular data have revealed a large diversity in the subunit composition of nAChRs in mammals which confers not only its biophysical characteristics but also its pharmacological profile. *In situ* hybridization studies in the spinal cord have revealed the presence of $\alpha 2$, $\alpha 3$, $\alpha 4$ and $\beta 2$ subunits in the central grey matter and only $\alpha 4$ and $\beta 2$ subunits in the IML (Wada *et al.* 1989). Seguela, Wadiche, Dineley-Miller, Dani & Patrick (1993) noted a moderate signal for $\alpha 7$ in the central grey matter of the spinal cord whereas no hybridization above background was detected for $\beta 4$ (Dineley-Miller & Patrick, 1992). One of the goals when establishing an order of potency of agonists and antagonists is to obtain some insight into the subunit composition of the receptors in comparison with the pharmacological profile of nAChR subunit combinations expressed in *Xenopus* oocytes (for review see McGehee & Role, 1995). It is worth noting that the pharmacology of the nicotinic receptor has been investigated in neurones showing detectable and measurable DMPP-induced inward currents. It is unlikely that homomeric $\alpha 7$ and $\alpha 3\beta 2$ nAChRs contributed to our recorded current because we found no effect of methyllycaconitine and neuronal bungarotoxin on DMPP-induced currents, respectively (for review see McGehee & Role, 1995). However, because of the slow agonist application used in our study and the rapid desensitization of the $\alpha 7$ response (Zhang, Vijayaraghavan & Berg, 1994), an $\alpha 7$ component may have escaped our investigation. The potency order of agonists (DMPP = nicotine > cytisine > ACh) found in neurones showing measurable currents in response to these agonists does not fit to any published potency order of various subunit combinations in *Xenopus* oocytes (for review see McGehee & Role, 1995). This, however, is not surprising if we simply consider that a neurone may express several nAChR subunits which assemble in a much more complex manner than in a *Xenopus* oocyte (Brussard, Yang, Doyle, Huck & Role, 1994; Conroy & Berg, 1995). Moreover, it is possible that we have underestimated the effect of ACh because it might be hydrolysed by endogenous acetylcholinesterase present in the slice. Alternatively Khan *et al.* (1994*a*, *b*) have suggested the presence of an atypical nAChR in spinal autonomic nuclei which could explain the non-blocking effect of hexamethonium in our preparation.

Nicotinic enhancement of glutamate-induced current. The nicotinic potentiation of glutamate-induced currents persisted in the presence of TTX, indicating a postsynaptic mechanism for this nicotinic effect, comparable with the recently reported effect of ATP on glutamate responses. We have not yet explored the mechanisms of this potentiation. DMPP can increase glutamate responses either by affecting the glutamate-binding affinity or by acting at a binding site closely associated with the glutamate–receptor complex or by triggering intracellular processes via activation of postsynaptic nAChRs onto presumed SPNs. Phosphorylations of glutamate receptors by protein kinases represent a major mechanism for regulation of their function (Roche, Tingley & Huganir, 1994). Since a Ca^{2+} chelator (EGTA) was used in our experiments, calcium-dependent phosphorylations are unlikely to explain the potentiation of glutamate responses. However, we cannot exclude this possibility for two reasons. Firstly, EGTA is a rather slow calcium buffer and secondly, glutamate may activate glutamate receptors located on distal dendrites possessing individual calcium compartments which are not fully buffered by EGTA. In addition, due to poor voltage control of distal dendrites, depolarization of distal dendrites by DMPP acting on postsynaptic nAChRs may remove the Mg^{2+} block of the NMDA receptors and then potentiate the glutamate response (for review see Edmonds, Gibbs & Colquhoun, 1995).

Presynaptic action of nicotinic agonist

Since no synaptic activity in neurones of the CA had been reported, we first described the spontaneous and electrically evoked synaptic activity observed in our study. We then evaluated the DMPP effect on this activity.

Excitatory transmission. Functional excitatory inputs into SPNs of the CA could be expected since supraspinal afferents from brain nuclei containing glutamate (Miura, Takayama & Okada, 1994) reach the CA (Ross, Ruggiero, Joh, Park & Reis, 1984; Mtui, Anwar, Gomez, Reis & Ruggiero, 1993). mRNAs of NMDA and α-amino-3-hydroxy-5-methylisoxazole-4-propionate/kainate subunits are expressed in the lamina X (Tölle, Berthele, Zieglgänsberger, Seeburg & Wisden, 1993). Indeed, our results show the presence of spontaneous and evoked excitatory synaptic events in 40% and in all recorded SPNs, respectively. The complete block by CNQX alone or in combination with APV and the reversal potential of the excitatory events as expected for a non-selective cationic conductance indicate that they were due to the activation of postsynaptic glutamate receptors. Several observations, such as the development of a second, slow component to the decay after depolarization and a region of negative slope conductance in the I–V relationship, suggest that the excitatory currents are due to the activation of both NMDA and non-NMDA receptors as commonly observed in the central nervous system (Edmonds *et al.* 1995; Krupp & Feltz, 1995).

The spontaneous EPSCs with a mean amplitude of −19·3 pA at a V_h of −50 mV are likely to be miniature sEPCSs. However, this assumption would need further confirmation in TTX-containing ACSF. The slower rise time of evoked EPSCs mediated by non-NMDA receptors (1·41 ± 0·28 ms for evoked EPSCs and 0·67 ± 0·06 ms for spontaneous EPSCs) is, as observed at cerebellar synapses (Silver, Traynelis & Cull-Candy, 1992), probably the result of an asynchronous release of multiple vesicles after an electrically induced action potential. This explanation can also account for the differences in the time course of current decay

(3·26 ± 0·14 *versus* 1·63 ± 0·44 ms for spontaneous EPSCs; Edmonds *et al.* 1995).

Nicotinic facilitation of excitatory synaptic transmission. In the brain, activation of presynaptic nAChRs has been reported to depress presynaptic action potentials recorded in the rat interpeduncular nucleus (Brown, Docherty & Halliwell, 1984), to facilitate spontaneous GABA release in the rat interpeduncular nucleus (Léna, Changeux & Mulle, 1993) and avian lateral spiriform nucleus (McMahon, Yoon & Chiappinelli, 1994) and to potentiate the evoked release of glutamate in the prefrontal cortex (Vidal & Changeux, 1993). Here, we have reported a facilitation of transmitter release (glutamate) by nAChR activation in the spinal cord. The site of action of nAChR agonist is presynaptic to the recorded neurones for two reasons. Firstly, DMPP caused an increase in the frequency of spontaneous EPSCs without necessarily having an effect on their amplitude. It also induced the appearance of spontaneous EPSCs in previously quiet neurones which suggests the activation of silent synapses. This idea is also supported by the decreased number of failures of evoked EPSCs after DMPP application as well as by the reduction in the latency of evoked EPSCs. Secondly, the increased frequency of sEPSCs and the increased amplitude of evoked EPSCs after application of DMPP were not accompanied by a detectable change in the decay time of both spontaneous and evoked EPSCs. This rules out the recruitment of latent NMDA receptors which would have decreased the decay time course (for review Edmonds *et al.* 1995). Therefore, nAChR agonists enhance the release of glutamate or an analogue substance by an unknown presynaptic mechanism, via activation of presynaptic nAChRs.

Functional implications and conclusions

One of the major actions of DMPP reported in this study is a direct depolarization of neurones in the CA which are presumed to be SPNs. SPNs of the CA send axons to several sympathetic ganglia and provide a particularly rich innervation of the inferior mesenteric ganglion (Strack, Sawyer, Marubio & Loewy, 1988). We, therefore, expect that nicotinic excitation of SPNs would lead to a direct modulation of the sympathetic outflow to peripheral ganglia. Such an excitatory action of nicotinic agonists is supported by a recent report showing the modulation of the sympathetic outflow *in vivo* following intrathecal administration of nAChR agonists by Khan *et al.* (1994*a*). The source of acetylcholine acting on SPNs of the CA is still unknown. Nevertheless, since no recurrent collaterals of SPNs have been reported in the CA (Hosoya *et al.* 1994), the cholinergic innervation of SPNs is more likely to be provided by interneurones of the lamina X. This region possesses the most widespread distribution of cholinergic neurones and terminals by comparison with other areas of the spinal cord (Barber *et al.* 1984). Moreover, Borges & Iversen (1986) have reported that neurones of the CA, presumably SPNs receive a cholinergic input from lamina X neurones. The second, presynaptic action of nicotinic agonists points to a more subtle modulatory control of the sympathetic outflow via enhancement of the excitatory neurotransmission onto SPNs. SPNs of the CA receive glutamatergic terminals from supraspinal origins (for review see Coote, 1988) and they are well positioned to receive excitatory inputs from the dorsal horn via an intraspinal relay which may convey nociceptive information (Nahin, Madsen & Giesler, 1983). These actions of nicotinic agonists emphasize the importance of a cholinergic network in the modulation of the sympathetic tone.

Alkondon, M., Pereira, E. F. R., Wonnacott, S. & Albuquerque, E. X. (1992). Blockade of nicotinic currents in hippocampal neurons defines methyllycaconitine as a potent and specific receptor antagonist. *Molecular Pharmacology* **41**, 802–808.

Barber, R. P., Phelps, P. E., Houser, C. R., Crawford, G. D., Salvaterra, P. M. & Vaughn, J. E. (1984). The morphology and distribution of neurons containing choline acetyltransferase in the adult rat spinal cord: an immunocytochemical study. *Journal of Comparative Neurology* **229**, 329–346.

Bordey, A., Feltz, P. & Trouslard, J. (1996). Patch-clamp characterization of nicotinic receptors in a subpopulation of lamina X neurones in rat spinal cord slices. *Journal of Physiology* **490**, 673–678.

Borges, L. F. & Iversen, S. D. (1986). Topography of choline acetyltransferase immunoreactive neurons and fibers in the rat spinal cord. *Brain Research* **362**, 140–148.

Brown, D. A., Docherty, R. J. & Halliwell, J. V. (1984). The action of cholinomimetic substances on impulse conduction in the habenulo-interpeduncular pathway of the rat *in vitro*. *Journal of Physiology* **353**, 101–109.

Brussaard, A. B., Yang, X., Doyle, J. P., Huck, S. & Role, L. W. (1994). Developmental regulation of multiple nicotinic AChR channel subtypes in embryonic chick habenula neurons: contributions of both the α_2 and α_4 subunits genes. *Pflügers Archiv* **424**, 27–43.

Conroy, W. G. & Berg, D. K. (1995). Neurons can maintain multiple classes of nicotinic acetylcholine receptors distinguished by different subunit compositions. *Journal of Biological Chemistry* **270**, 4424–4431.

Coote, J. H. (1988). The organization of cardiovascular neurons in the spinal cord. *Review of Physiology and Biochemical Pharmacology* **110**, 147–285.

Coote, J. H., Macleod, V. H., Fleetwood-Walker, S. & Gilbey, M. P. (1981). The response of individual sympathetic preganglionic neurones to microelectrophoretically applied endogenous monoamines. *Brain Research* **215**, 135–145.

Dineley-Miller, K. & Patrick, J. (1992). Gene transcripts for the nicotinic acetylcholine receptor subunit, $\beta 4$, are distributed in multiple areas of the rat central nervous system. *Molecular Brain Research* **16**, 339–344.

Eccles, J. C., Fatt, P. & Koketsu, K. (1954). Cholinergic and inhibitory synapses in a pathway from motor-axon collaterals to motoneurones. *Journal of Physiology* **126**, 524–562.

Edmonds, B., Gibbs, A. J. & Colquhoun, D. (1995). Mechanisms of activation of glutamate receptors and the time course of excitatory synaptic currents. *Annual Review of Physiology* **57**, 495–519.

Grace, A. A. & Llinas, R. (1985). Morphological artifacts induced in intracellularly stained neurons by dehydration: circumvention using rapid dimethyl sulfoxide clearing. *Neuroscience* **16**, 461–475.

HOSOYA, Y., NADELHAFT, I., WANG, D. & KHONO, K. (1994). Thoracolumbar sympathetic preganglionic neurons in the dorsal commisural nucleus of the male rat: an immunohistochemical study using retrograde labeling of cholera toxin subunit B. *Experimental Brain Research* **98**, 21–30.

INOKUCHI, H., MASUKO, S., CHIBA, T., YOSHIMURA, M., POLOSA, C. & NISHI, S. (1993). Membrane properties and dendritic arborization of the intermediolateral nucleus neurons in the guinea-pig thoracic spinal cord *in vitro*. *Journal of the Autonomic Nervous System* **43**, 97–106.

KHAN, I. M., TAYLOR, P. & YAKSH, T. L. (1994*a*). Cardiovascular and behavioral responses to nicotinic agents administrated intrathecally. *Journal of Pharmacology and Experimental Therapeutics* **270**, 150–158.

KHAN, I. M., YAKSH, T. L. & TAYLOR, P. (1994*b*). Ligand specificity of nicotinic acetylcholine receptors in rat spinal cord: studies with nicotine and cytisine. *Journal of Pharmacology and Experimental Therapeutics* **270**, 159–166.

KRUPP, J. & FELTZ, P. (1993). Synaptic- and agonist-induced chloride currents in neonatal rat sympathetic preganglionic neurons *in vitro*. *Journal of Physiology* **471**, 729–748.

KRUPP, J. & FELTZ, P. (1995). Excitatory postsynatic currents and glutamate receptors in neonatal rat sympathetic preganglionic neurons *in vitro*. *Journal of Neurophysiology* **73**, 1503–1512.

LÉNA, C., CHANGEUX, J.-P. & MULLE, C. (1993). Evidence for 'preterminal' nicotinic receptors on GABAergic axons in the rat interpeduncular nucleus. *Journal of Neuroscience* **13**, 2680–2688.

LLANO, I., MARTY, A., ARMSTRONG, C. M. & KONNERTH, A. (1991). Synaptic- and agonist-induced currents of Purkinje cells in rat cerebellar slices. *Journal of Physiology* **434**, 183–213.

MCGEHEE, D. S. & ROLE, L. W. (1995). Physiological diversity of nicotinic acetylcholine receptors expressed by vertebrate neurons. *Annual Review of Physiology* **57**, 521–546.

MCMAHON, L. L., YOON, K.-W. & CHIAPPINELLI, V. A. (1994). Nicotinic receptor activation facilitates GABAergic neurotransmission in the avian lateral spiriform nucleus. *Neuroscience* **59**, 689–698.

MIURA, M., TAKAYAMA, K. & OKADA, J. (1994). Distribution of glutamate- and GABA-immunoreactive neurons projecting to the cardioacceloratory center of the intermediolateral nucleus of the thoracic cord of SHR and WKY rats: a double-labeling study. *Brain Research* **638**, 139–150.

MTUI, E. P., ANWAR, M., GOMEZ, R., REIS, D. J. & RUGGIERO, D. A. (1993). Projections from the nucleus tractus solitarii to the spinal cord. *Journal of Comparative Neurology* **337**, 231–252.

MYSLINSKI, N. R. & RANDIĆ, M. (1977). Responses of identified spinal neurones to acetylcholine applied by micro-electrophoresis. *Journal of Physiology* **269**, 195–219.

NAHIN, R. L., MADSEN, A. M. & GIESLER, G. J. (1983). Anatomical and physiological studies of the gray matter surrounding the spinal cord central canal. *Journal of Comparative Neurology* **220**, 321–335.

PERRINS, R. & ROBERTS, A. (1994). Nicotinic and muscarinic receptors in rhythmically active spinal neurones in the *Xenopus laevis* embryo. *Journal of Physiology* **478**, 221–228.

ROCHE, K. W., TINGLEY, W. G. & HUGANIR, R. L. (1994). Glutamate receptor phosphorylation and synaptic plasticity. *Current Opinion in Neurobiology* **4**, 383–388.

ROSS, C. A., RUGGIERO, D. A., JOH, T. H., PARK, D. H. & REIS, D. J. (1984). Rostral ventrolateral medulla: selective projections to the thoracic autonomic cell column from the region containing C1 adrenaline neurons. *Journal of Comparative Neurology* **228**, 168–185.

SEGUELA, P., WADICHE, J., DINELEY-MILLER, K., DANI, J. A. & PATRICK, J. W. (1993). Molecular cloning, functional properties, and distribution of rat brain $\alpha 7$: a nicotinic cation channel highly permeable to calcium. *Journal of Neuroscience* **13**, 596–604.

SHERRIF, F. E. & HENDERSON, Z. (1994). A cholinergic propriospinal innervation of the rat spinal cord. *Brain Research* **634**, 150–154.

SILVER, R. A., TRAYNELIS, S. F. & CULL-CANDY, S. G. (1992). Rapid time-course miniature and evoked excitatory currents at cerebellar synapses *in situ*. *Nature* **355**, 163–166.

STRACK, A. M., SAWYER, W. B., MARUBIO, L. M. & LOEWY, A. D. (1988). Spinal origin of sympathetic preganglionic neurons in the rat. *Brain Research* **455**, 187–191.

TÖLLE, T. R., BERTHELE, A., ZIEGLGÄNSBERGER, W., SEEBURG, P. H. & WISDEN, W. (1993). The differential expression of 16 NMDA and non-NMDA receptor subunits in the rat spinal cord and in periaqueductal gray. *Journal of Neuroscience* **13**, 5009–5028.

URBAN, L., WILLETTS, J., MURASE, K. & RANDIĆ, M. (1989). Cholinergic effects on spinal dorsal horn neurons *in vitro*: an intracellular study. *Brain Research* **500**, 12–20.

VIDAL, C. & CHANGEUX, J.-P. (1993). Nicotinic and muscarinic modulations of excitatory synaptic transmission in the rat prefrontal cortex *in vitro*. *Neuroscience* **56**, 23–32.

WADA, E., WADA, K., BOULTER, J., DENERIS, E., HEINEMANN, S., PATRICK, J. & SWANSON, L. W. (1989). Distribution of $\alpha 2$, $\alpha 3$, $\alpha 4$, and $\beta 2$ neuronal nicotinic receptor subunit mRNAs in the central nervous system: a hybridization histochemical study in the rat. *Journal of Comparative Neurology* **284**, 314–335.

YOSHIMURA, M. & NISHI, S. (1982). Intracellular recordings from lateral horn cells of the spinal cord *in vitro*. *Journal of the Autonomic Nervous System* **6**, 5–11.

ZHANG, Z. W., VIJAYARAGHAVAN, S. & BERG, D. K. (1994). Neuronal acetylcholine receptors that bind alpha-bungarotoxin with high affinity function as ligand-gated ion channels. *Neuron* **12**, 167–177.

Acknowledgements

This study was supported by CNRS, Université Louis Pasteur, INSERM and Direction des Recherches et Techniques. We thank Drs J. Krupp, S. J. Marsh and J. Sim for their constructive comments.

Author's email address

J. Trouslard: Trouslard@neurochem.u-strasbg.fr

Received 18 September 1995; accepted 25 July 1996.